Proceedings of the
Annual Stability Conference
Structural Stability Research Council
Charlotte, North Carolina, April 11-14, 2023

Local buckling and design of aluminum I-shapes

Tristan Coderre[1], Liya Li[2], Sahar Dahboul[3], Nicolas Boissonnade[4]

Abstract

Current standards use simplified approaches to predict the resistance of aluminum elements that are not optimized to account for the effects of strain hardening, instabilities, and heat reduced properties. This paper summarizes investigations towards the development of an alternative design method for aluminum open cross-sections, based on the Overall Interaction Concept (O.I.C.). This innovative design approach relies on the interaction between resistance and stability, and also allows to consider geometrical and material imperfections. Moreover, it allows to obtain direct, precise and consistent resistance predictions using continuous buckling curves.

A numerical finite element model was developed to accurately predict the cross-sectional resistance of aluminum elements. Its efficiency was validated by comparing its numerical resistance predictions to available experimental test data. Extensive parametric studies were then conducted, allowing to study the impact of varying geometries, alloys, and load cases on the resistance. Using the results from more than 2 300+ numerical simulations, O.I.C.-type design proposals were formulated for the local resistance of extruded and welded aluminum sections.

The performance of the design proposals was evaluated by comparing their resistance estimates to the reference numerical results and to resistance predictions from the Canadian, European, and American aluminum design standards. The comparisons showed that the O.I.C. design proposal leads to much more accurate and consistent results than these standards, while remaining simpler and more efficient.

1. Introduction

The present paper addresses the behaviour, structural response and resistance of aluminium I-shapes – either extruded or welded – under simple or combined load cases. Albeit marginally used for heavy Structural Engineering applications, aluminium structural elements are gaining interest owing to (i) an outstanding strength-to-weight ratio, (ii) its resistance to corrosion, in particular in severe humidity and industrial conditions, considerably reducing maintenance costs, (iii) great recycling abilities, (iv) an original manufacturing process (extrusion) complementary

[1] MSc student, Laval University, <tristan.coderre.1@ulaval.ca>
[2] Post-Doc student, Laval University, <liya.li.1@ulaval.ca>
[3] PhD student, Laval University, <sahar.dahboul.1@ulaval.ca>
[4] Professor, Laval University, <nicolas.boissonnade@gci.ulaval.ca>

to more "traditional" ones (welding) and (v) stable resistance and ductility properties even at very low temperatures, which shows particularly suitable in northern climates. All these qualities leads to an increased use of aluminium members in construction projects, which causes an improving need for suitable and economic modern design rules.

Nevertheless, most of the current design rules relative to aluminium structures (Aluminum Association 2020; Canadian Standards Association 2017; European Committee for Standardization 2007), usually based on steel structures' codes, suffer a series of problems, from a general lack of knowledge to inaccuracies. Among them, the underlying assumption of a plastic plateau in the material response can be shown the source of many over-conservative resistance predictions. Too, oversimplified, linear design equations appear poorly suited to aluminium extruded shapes, which usually exhibit very complex geometries (Extrudex Aluminium Inc. 2020; Metra Aluminium Inc. 2019; Sapa Inc. 2008). Aluminium remaining a costly material, it is therefore necessary to improve current design approaches in order to guarantee optimized designs, to accurately consider the non-linear material response, to increase resistance predictions accuracy, and to simplify the design process.

In this respect, this paper summarizes research efforts undertaken towards an improved, more adequate design approach for aluminium structural sections, specifically for I-shaped sections. The proposed approach is based on the Overall Interaction Concept (O.I.C., (Beyer 2017; Boissonnade et al. 2017; Gagné et al. 2020; Gérard et al. 2021; Li et al. 2022)); the latter, initially developed for steel members, is extended to aluminium shapes and accounts for (i) a realistic stress-strain relationship, (ii) I-shapes form either extrusion or welding processes and (iii) compact as well as slender geometries. The accuracy and performance of the proposal is tested against reference Finite Element (F.E.) results. The non-linear shell models on which the numerical studies rely are detailed in Section 2; in particular, the F.E. models are validated against experimental tests on I-shaped specimens performed by Yuan (Yuan et al. 2015) in Section 2.2. Then, a series of numerical computations varying the shapes, alloys and load combinations are performed (Section 2.3). Next, Section 3 details the proposed O.I.C.-based approach for both extruded and welded shapes. It further assesses the merits of this approach against the reference numerical results and against existing design provisions from Eurocode 9 (European Committee for Standardization 2007), from the Aluminium Design Manual (A.D.M., Aluminum Association 2020), and from the Canadian Standard S157 (Canadian Standards Association 2017).

2. F.E. models: development, validation and parametric studies

2.1 Basic features

Non-linear shell F.E. models were developed within software ABAQUS (Abaqus 2011). Typical S4R quadrangular 4 nodes shell elements relying on Kichhoff's bending assumptions combined with reduced integration were used and placed at mid-thickness of each plate element within the I-sections. Both Linear Buckling Analyses (L.B.A.), M.N.A. (Materially Non-linear Analyses) and G.M.N.I.A. (Geometrically and Materially Non-linear with Imperfection Analyses) computations were performed, providing accurate information on respectively buckling, yielding and ultimate responses of the aluminium sections. State-of-the-art numerical techniques have been employed, such as the subspace iteration method for L.B.A. (Bathe 2016), the Riks Method for G.M.N.I.A. (Riks 1979), automatic loading strategies (Abaqus 2011), etc.

The section modelling of extruded sections was the subject of specific attention with respect to web-flange areas, as extra material in the flange fillets can be shown to provide a non negligible influence on resistance (Gérard et al. 2019; Gérard et al. 2021; Guo 1989; Li et al. 2022). In these areas, two "problems" arise: (i) an overlap of material and (ii) the fact that the fillets' areas are not included. Accordingly, extra beam elements were introduced and positioned at the centroid of the radius zone (see Figure 1). The area of these elements is set equal to the radius area minus the overlapping area, and their section shape is chosen to be a square hollow section so as to match all geometrical properties, and in particular closely represent torsional rigidities.

Besides, since an accurate representation of local buckling is important in the present study, a truss system was added to the F.E. models to characterize the actual behavior of the web-flange zone and its impact on the section's response to buckling. The truss system, modelled through relatively stiff spring elements, allows to maintain this area undeformed so that local buckling in the adjacent web/flange plates initiates at the foot of the radius, similarly to the real section.

For the welded shapes considered herein, no such modelling refinements were adopted since welds do not provide a meaningful effect on resistance. Yet, specific material properties in the Heat-Affected Zone (H.A.Z.) were considered (Coderre 2022).

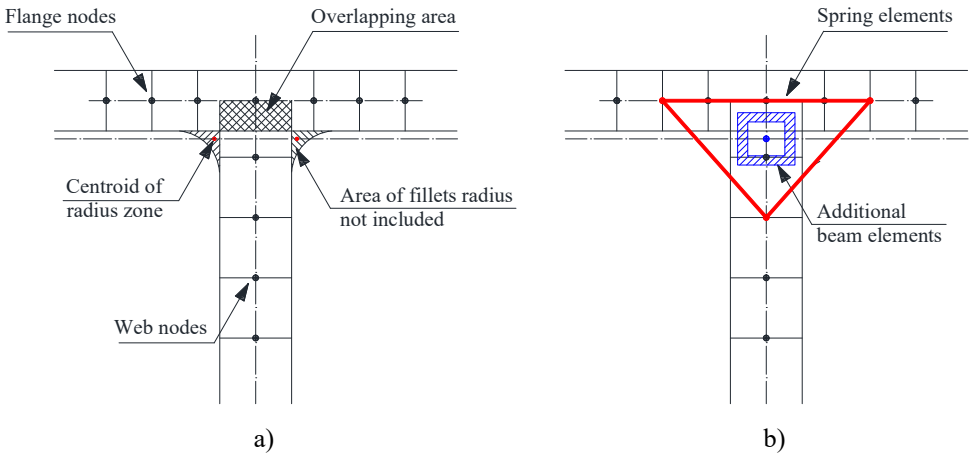

Figure 1: Modelling of web-flange area for extruded sections − a) Real geometry − b) Modelled geometry.

Obviously, mesh density studies were performed prior to any use of the numerical models, the goal being to find the best compromise between a sufficient accuracy and a reasonable computation time (details can be found in Coderre 2022). Figure 2 shows various mesh densities used beforehand when searching for the most suitable mesh density. Results were typically G.M.N.I.A. computations on a regular computer, and Figure 3 proposes an example of results obtained for ultimate loads of sections in compression or under major-axis bending moment M_y. It is observed that Types I-III usually keep a G.M.N.I.A. computation below 5 min and that Type V may reach up to 20 min calculation time. In terms of precision, Types III and IV meshes have been shown to lead to results with a difference lower than 3% compared to Type V taken as a reference. Accordingly, Type III mesh was selected for all F.E. calculations, namely within numerical parametric studies (Section 2.3), for both extruded and welded sections.

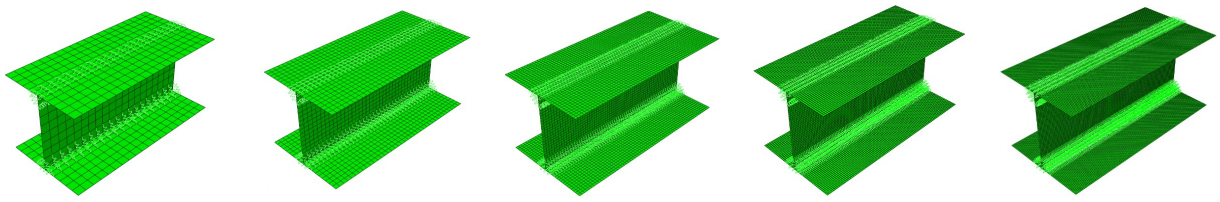

Figure 2: Various mesh densities studied, from coarser (Type I) to finer (Type V).

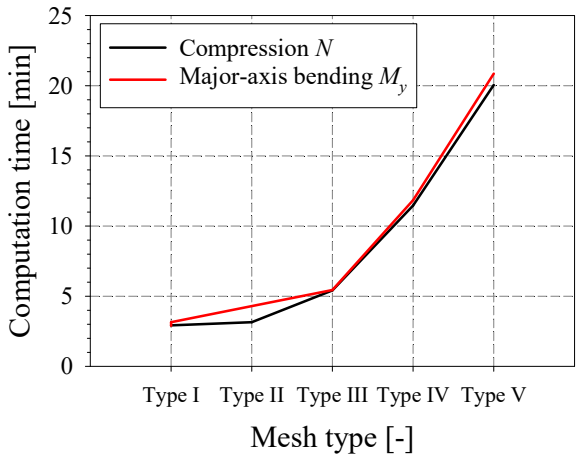

Figure 3: Average computation time for G.M.N.I.A. calculations for the various meshes considered.

To adequately represent the material response of aluminium, stress-strain relationships followed the so-called "Ramberg-Osgood equation" (Ramberg and Osgood 1943), which has further been modified by Hill to take into account permanent deformation using the offset method (Hill, 1944), as presented in Eq. (1). This material model was used in all calculations, and alloys 6061-T6, 6063-T6 and 6082-T6 were considered – the latter can indeed be shown to be the most representative ones for Structural Engineering applications.

$$\varepsilon = \frac{\sigma}{E} + 0.002\left(\frac{\sigma}{F_y}\right)^n \tag{1}$$

Following the recommendations of most design standards, the Youngs' modulus was fixed as $E = 70\,000$ N/mm^2 and the remaining values needed in Eq. (1) were set according to Canadian Standards' S157 (namely exponent n), see Table 1 (Coderre 2022).

Table 1: Properties of the aluminium alloys used in Ramberg-Osgood equations.

	Non H.A.Z.			H.A.Z.		
Alloy	F_y [N/mm^2]	F_u [N/mm^2]	n [-]	F_{wy} [N/mm^2]	F_{wu} [N/mm^2]	n [-]
6061-T6	240	260	55	105	165	8.1
6063-T6	170	205	19.5	55	115	-
6082-T6	260	310	20.7	110	190	6.7

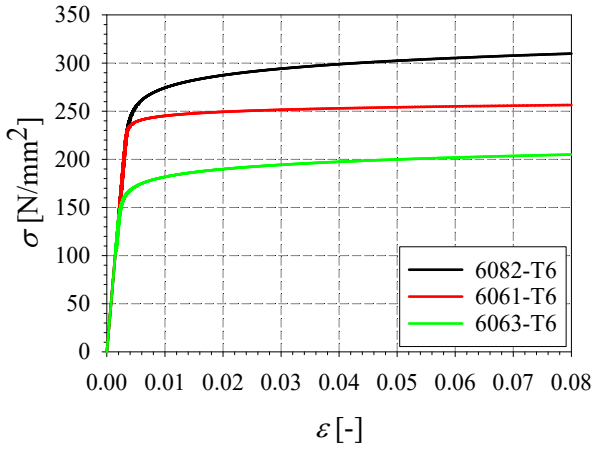

Figure 4: Stress-strain relationships for the various alloys considered.

Figure 4 presents the resulting σ-ε curves obtained for the different aluminium alloys that were considered herein, namely along the parametric studies. They have been introduced in the F.E. models by means of a total of 100 σ-ε pairs spanning the entire material response. This number of points has proven to be sufficient to accurately represent the behavior of non-linear materials in the numerical model (Gagné 2022; Coderre 2022).

Material imperfections have not been accounted for in models relative to extruded sections. According to studies conducted by Mazzolani (Mazzolani 1994), residual stresses in extruded aluminium products – irrespective of the shape or the heat-treatment – are usually pretty low and have an insignificant effect of the load-bearing capacity (Mazzolani 1994; Coderre 2022).

Yet, residual stresses patterns as in Figure 5b were considered for welded profiles, following Kristensen's study on 6082-T6 aluminium sections (Kristensen and Moan 1999). This distribution is also very similar to the patterns used by Zha and Moan (Zha and Moan 2001; Zha and Moan 2003) and by Rigo et al. (Rigo et al. 2003). The compressive residual stresses, σ_c were carefully calculated so that every plate respects a self-equilibrium condition between tensile and compressive stresses; also, note that reductions in mechanical properties in the H.A.Z. have also been taken into account in the F.E. models, by carefully modifying node coordinates, allowing to precisely align the end of the shell elements with the extent of each zone (Coderre 2022). Finally, careful numerical checks have been conducted to confirm that the introduction of this residual stresses pattern was indeed leading to patterns in self-equilibrium (Coderre 2022).

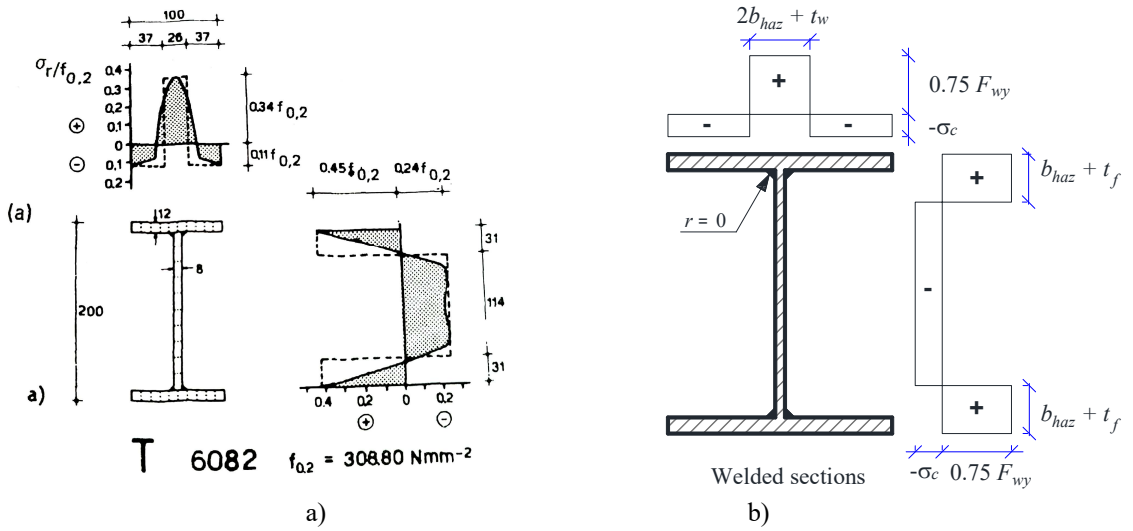

a) b)

Figure 5: Residual stresses patterns – a) Measured by Mazzolani (Mazzolani 1994) – b) Considered in the F.E. models for welded sections.

The support conditions of the F.E. models were defined as ideal fork conditions, meaning that axial displacement, strong axis rotation, weak axis rotation, and warping were allowed. To achieve these conditions, specific degrees of freedom of both ends' nodes were constrained. The nodes of the flanges and of the web were restrained in the direction perpendicular to their plane, which also prevented local buckling of the plates that could occur due to stress concentrations at load application areas. Rotation about the longitudinal axis was restrained at the four nodes directly at the web-to-flange junctions, in order to prevent torsion and out of plane rotation. Axial displacements were also fixed at the middle node of the (short) member to allow both ends to move towards or away from this point. The boundary conditions applied to the model are schematically represented in Figure 6a.

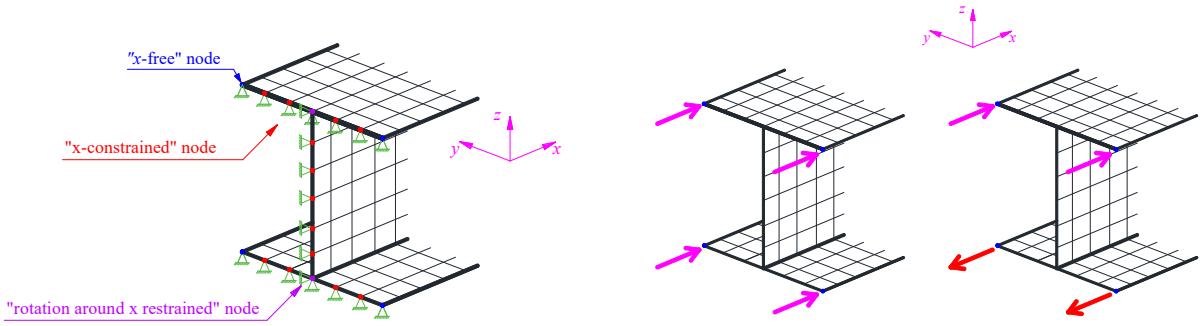

a) b)

Figure 6: Boundary condition and load application − a) Modelling of end sections: transverse supports and constraints conditions − b) Application of compression or major-axis bending through nodal forces.

Further, to guarantee that beam theory assumptions were effectively fulfilled ("plane sections remain plane"), kinematic linear constraints were applied to the nodes of the end sections (Figure 6a). With these constraints, the axial displacement of each node was controlled by the four corner nodes, i.e., the nodes at the flanges' tips. This also allowed the different loads used in the study – compression (N), major axis bending (M_y), and minor axis bending (M_z) – to be applied as punctual loads acting axially on the corner nodes, see Figure 6b.

Initial geometrical imperfections were also considered in the numerical models, through adequately modifying nodes coordinates. Typical patterns adopted are schematically represented in Figure 7 and follow sinusoidal distributions; 3 half-waves in each plate have been considered, the half-wave length being defined as the average between the flat "local buckling length" of the flange a_f and its web counterpart a_w. Each plate was assigned an imperfection's amplitude as $1/200^{th}$ of either a_f or a_w – several variations relative to the shape of the imperfections or their amplitudes have been studied beforehand and led to the values proposed here (Coderre 2022).

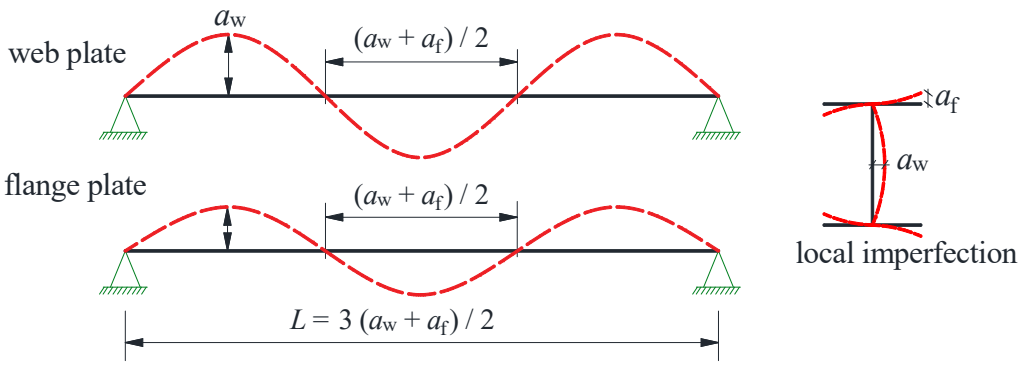

Figure 7: Sine-shaped geometrical imperfections in web and flange plates.

2.2 Validation against experimental results

Analyses performed thanks to the numerical model were compared to experimental test results on the local behavior of aluminium I-sections found in the literature. In this respect, the experimental results from Yuan et al. on stub columns (Yuan et al. 2015) have been used for validation purposes. All test specimens were fabricated from extrusion, and no radius area was present. Obviously, all *measured* material and geometrical data have been implemented in the numerical models, as reported in Table 2 and Table 3. Further, for each test specimen, Yuan et al. measured the initial local geometrical imperfections at three regions of the cross-sections: one at mid-length (section B), and the others close to both ends (sections A and B). Figure 8a and Figure 8b illustrate the imperfections' distribution pattern of specimens T6-300-200 and T5-240-75. The schematic view of the imperfections and their amplitude is also shown.

On the basis of Figure 8, it was chosen in the validation studies to implement the initial local geometrical imperfections as a single sinusoidal half-wave, coupled with the measured amplitudes in each plate. The direction of the imperfections was based on the schematic view of Figure 8c, and the measured amplitudes are reported in Table 2.

Table 2: Measured geometrical properties of specimens and test vs F.E. results.

Specimen	Alloy	Die toolset	h [mm]	b [mm]	t_f [mm]	t_w [mm]	L [mm]	*Geom. imp. web* [mm]	*Geom. imp. flange* [mm]	$N_{u,Exp.}$ [kN]	$N_{u,F.E.}$ / $N_{u,Exp.}$ [–]
T6-300-150	6061-T6	1	300.1	149.4	10.89	7.79	897.9	0.09	-0.07	1353.0	1.05
T6-300-200		1	300.1	199.2	10.87	7.67	899.4	-0.52	-0.13	1569.5	1.03
T6-280-160-R		2	279.5	159.4	9.9	6.94	839.8	0.27	0.17	1139.6	1.07
T6-350-110-R		3	349.3	111	10.06	7.72	1052.9	0.39	0.09	1057.8	0.90
T6-350-150-R		3	350.7	149.9	10.01	7.95	1049.4	-0.40	0.18	1271.0	0.96
T6-350-200-R		3	350.6	199.8	10	7.93	1049.8	-0.42	0.13	1442.2	0.98
T6-450-150-R		4	449.5	147.4	10.21	8.4	1351.5	1.45	0.08	1135.7	0.95
T6-450-200-R		4	449.9	199.7	10.5	8.64	1348.1	1.03	-0.33	1365.1	1.03
T5-240-75	6063-T5	5	239.8	74.7	6.96	4.44	719.6	-0.51	-0.19	254.1	0.93
T5-240-118		5	239.8	117.3	6.9	4.35	720.3	0.39	-0.22	340.2	0.98
T5-240-168		5	239.3	168.7	7	4.25	720.3	0.38	-0.24	446.8	0.91
T5-240-208		5	239	206.9	6.92	4.11	719.6	0.27	-0.49	520.6	0.83
T5-270-100		6	269.1	100.3	5.96	3.59	809.1	0.30	-0.21	295.1	0.91
T5-270-145		6	269.3	144.5	5.96	3.64	808.6	-0.23	-0.18	315.6	1.07
T5-270-178		6	268.9	178.0	5.83	3.63	809.0	0.30	-0.33	332.0	1.07
										Mean	0.98
										C.O.V.	0.08

Table 3: Measured material properties of specimens.

Alloy	Die toolset	Location	E [N/mm^2]	F_y [N/mm^2]	F_u [N/mm^2]	n [–]
6061-T6	1	Flange	70 100	279.9	296.2	28.0
		Web	68 900	258.1	289.7	25.8
	2	Flange	72 600	257.8	291.5	25.8
		Web	70 000	270.5	298.5	27.1
	3	Flange	70 800	248.0	285.6	24.8
		Web	72 500	264.8	297.9	26.5
	4	Flange	68 300	231.7	260.6	23.2
		Web	69 100	249.7	291.4	25.0
6063-T5	5	Flange	63 300	142.5	185.3	14.2
		Web	67 200	154.6	201.6	15.5
	6	Flange	63 700	170.2	215.6	17.0
		Web	64 600	168.4	218.0	16.8

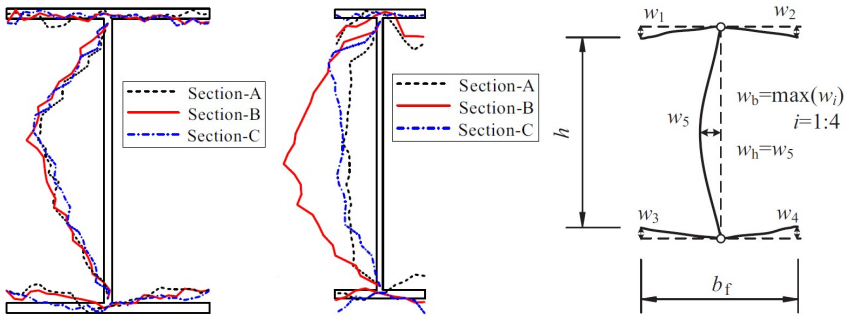

a) b) c)

Figure 8: Measured local imperfections from (Yuan et al. 2015) − a) Distribution pattern for specimen T6-300-200 – b) Distribution pattern for specimen T5-240-75 – c) Schematic view.

The experimental setup, in particular the support conditions, were recreated numerically as accurately as possible (fixed ends with warping restrained, end rotations prevented). Table 2 reports the results obtained for each specimen and allows comparing each test result with its numerically-predicted counterpart. Overall, the numerical results are seen to be in quite good agreement with the experimental sources and are usually safe-sided. In average, some 2% difference between sources is reported, with a Coefficient of Variation (C.O.V.) of 0.08, which is excellent. As a complement, Figure 9a provides examples of typical stress-strain cures (obtained from load-displacement data) where a good correspondence between the numerical sources and the reference test data is observed, in terms of peak load, initial stiffness, post peak behaviour, etc. Figure 9b further illustrates the similarities between experimental and numerical failure modes. Accordingly, the F.E. models are deemed fit for being substituted to physical testing and have been thoroughly used within numerical parametric studies, as detailed in the next paragraphs.

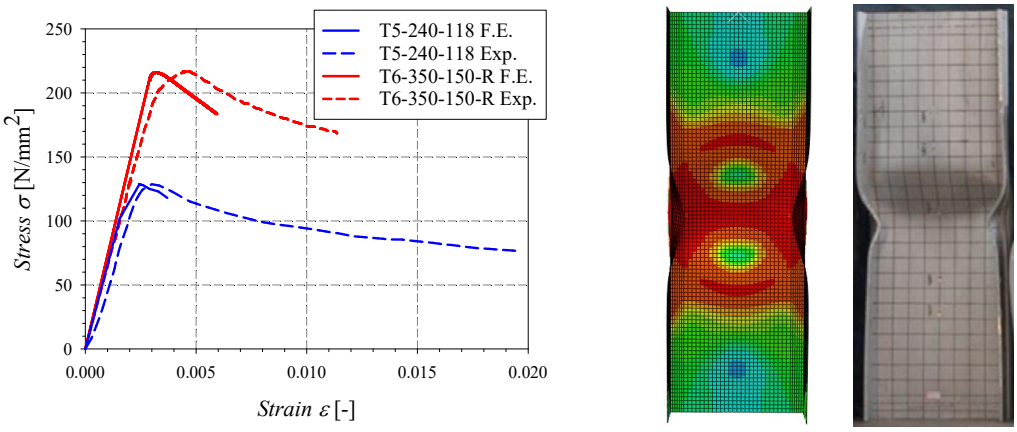

a) b)

Figure 9: Examples of test vs F.E. − a) Load-displacement curves − b) Failures modes.

2.3 Parametric studies

The numerical models being validated, large amounts of both L.B.A. and G.M.N.I.A. numerical simulations were performed to collect information on (i) the critical buckling response of such aluminium I-shaped sections and on (ii) their ultimate (failure) loads, respectively. Overall, some 2 368 non-linear shell F.E. computations have been performed, with the following parameters being varied:

- Cross-section types and shapes (Table 5): 30 I-shaped extruded sections selected from Canadian and American extruders' sections catalogs as well as 29 welded aluminium cross-sections inspired by bridge girders (designation starts with "BG"), column shapes ("HEA") or invented sections ("IS") have been considered;
- 3 different heat-treated aluminium alloys: alloys 6061-T6 (F_y = 240 N/mm^2), 6082-T6 (F_y = 260 N/mm^2) and 6063-T6 (F_y = 170 N/mm^2). Only the first 2 alloys wee considered for welded sections, owing to limitations in fabrication and in welded area performance;
- Multiple load cases: axial compression N, major-axis bending M_y, minor-axis M_z and a series of combined loading situations as characterized by Figure 13 and Table 4 (further explanations on Figure 13 are given later in the paper).

$$n = N/N_{pl} = N/\left(A \cdot F_y\right) \tag{2}$$

$$m_y = M_y/M_{pl,y} = M_y/\left(W_{pl,y} \cdot F_y\right) \tag{3}$$

$$m_z = M_z/M_{pl,z} = M_z/\left(W_{pl,z} \cdot F_y\right) \tag{4}$$

$$\tan\theta = m_y/\left(n \cdot \cos\varphi\right) = m_z/\left(n \cdot \sin\varphi\right) \tag{5}$$

$$\tan\varphi = m_z/m_y \tag{6}$$

Table 4: Combined load cases considered in this study.

φ [°]	n [–]	Load case
0	0.4	$N + M_y$
	0.8	$N + M_y$
30	0	$M_y + M_z$
	0.4	$N + M_y + M_z$
	0.8	$N + M_y + M_z$
50	0	$M_y + M_z$
	0.4	$N + M_y + M_z$
	0.8	$N + M_y + M_z$
70	0	$M_y + M_z$
	0.4	$N + M_y + M_z$
	0.8	$N + M_y + M_z$
90	0.4	$N + M_z$
	0.8	$N + M_z$

Table 5: Chosen cross-sections for parametric studies.

Manufacturing	Cross-section	h [mm]	b [mm]	t_f [mm]	t_w [mm]	r [mm]	b / t_f [–]	h / t_w [–]
Extruded shapes	I3x2	76.20	63.50	6.35	4.78	9.53	5.0	14.6
	I3x2-	76.20	63.50	5.00	3.76	6.27	6.4	18.9
	S687	76.20	50.80	6.35	4.78	9.53	4.0	14.6
	MS186	95.25	30.15	3.18	1.83	1.65	4.7	50.3
	I4x2	101.60	76.20	6.35	4.78	9.53	6.0	19.9
	I4x2-	101.60	76.20	12.00	9.02	9.53	3.2	9.9
	S181	101.60	53.98	3.81	4.06	3.81	7.1	24.1
	S208	111.13	50.80	6.35	6.35	6.35	4.0	16.5
	I6x4	152.40	101.60	7.37	4.83	7.62	6.9	30.0
	I6x5-	152.40	101.60	16.00	10.48	7.62	3.2	13.0
	I6x4-	152.40	101.60	6.00	3.93	6.21	8.5	37.3
	WF6x9	152.40	152.40	12.70	9.53	15.88	6.0	14.7
	I7x5	177.80	101.60	9.53	7.14	11.13	5.3	23.6
	I7x5-	177.80	101.60	6.50	4.87	7.59	7.8	35.2
	I8x6	203.20	101.60	9.53	7.14	11.10	5.3	27.1
	I8x6-	203.20	101.60	6.00	4.50	6.99	8.5	43.8
	S263	203.20	133.35	7.82	5.84	8.13	8.5	33.5
	S263-	203.20	133.35	6.50	4.85	6.75	10.3	40.6
	I6x9-	203.20	203.20	12.70	9.53	15.88	8.0	20.0
	I10x9-	254.00	127.00	8.75	6.00	9.83	7.3	40.9
	I10x11	254.00	152.40	12.70	9.53	14.27	6.0	25.3
	I10x11-	254.00	152.40	11.33	8.50	14.27	6.7	28.5
	I8x7-	254.00	127.00	9.53	7.14	11.10	6.7	34.2
	I10x11--	254.00	152.40	7.00	4.27	6.83	10.9	57.8
	I12x15	304.80	165.10	15.88	11.10	15.88	5.2	26.0
	I12x15-	304.80	165.10	14.30	10.00	14.30	5.8	29.1
	I12x14	304.80	177.80	15.75	7.87	10.16	5.6	36.7
	I12x14-	304.80	177.80	12.00	6.00	7.74	7.4	48.8
	I14x16	355.60	203.20	15.24	7.62	10.16	6.7	44.7
	I14x16-	355.60	203.20	11.00	5.50	7.33	9.2	62.7
Welded shapes	BG390	390.00	300.00	35.60	20.60	0.00	4.2	17.2
	BG500	500.00	250.00	42.90	10.70	0.00	2.9	42.7
	BG500-	500.00	250.00	57.10	14.30	0.00	2.2	31.0
	BG600	600.00	250.00	28.60	19.10	0.00	4.4	29.9
	BG600-	600.00	250.00	22.90	15.30	0.00	5.5	37.7
	BG800	800.00	300.00	34.30	17.10	0.00	4.4	44.8
	BG900	900.00	400.00	57.10	28.60	0.00	3.5	29.5
	BG900-	900.00	300.00	42.90	22.90	0.00	3.5	37.4
	BG1000	1000.00	400.00	57.10	22.90	0.00	3.5	41.2
	BG1100	1100.00	400.00	57.10	28.60	0.00	3.5	36.5
	BG1100-	1100.00	400.00	45.70	22.90	0.00	4.4	46.0
	BG1200	1200.00	500.00	71.40	28.60	0.00	3.5	39.5
	BG1200-	1200.00	500.00	57.10	22.90	0.00	4.4	49.9
	HEA100-	192.00	200.00	16.00	10.00	0.00	6.3	17.6
	HEA120-	228.00	240.00	16.00	10.00	0.00	7.5	21.2
	HEA140-	199.50	210.00	19.10	12.40	0.00	5.5	14.5
	HEA180-	213.80	225.00	11.90	7.50	0.00	9.5	26.9
	HEA220	210.00	220.00	11.00	7.00	0.00	10.0	28.4
	HEA260-	250.00	260.00	16.30	9.80	0.00	8.0	23.8
	HEA320	310.00	300.00	15.50	9.00	0.00	9.7	32.7
	HEA320-	310.00	300.00	20.20	11.70	0.00	7.4	24.8
	HEA450-	440.00	300.00	27.30	15.00	0.00	5.5	27.5
	HEA550	540.00	300.00	24.00	12.50	0.00	6.3	41.3
	HEA550-	540.00	300.00	36.00	18.80	0.00	4.2	26.8
	IS7x5	177.80	101.60	6.50	4.90	0.00	7.8	35.0
	IS263	203.20	133.35	6.50	4.90	0.00	10.3	40.1
	IS10x9	254.00	152.40	7.00	4.30	0.00	10.9	57.4
	IS12x14	304.80	177.80	12.00	6.00	0.00	7.4	48.8
	IS14x16	355.60	203.20	11.00	5.50	0.00	9.2	62.7

3. Proposed O.I.C.-based design approach

3.1 Bases and background

The F.E. results have served as reference to assess the merits of a new design procedure based on the O.I.C. approach (results in Section 3.2 and in Section 3.3). The O.I.C. method relies on the definition of a relative slenderness – denoted here as $\overline{\lambda}_L$ for *local* (cross-sectional) resistance – that takes the balance between plastic resistance and the section's local instability. After $\overline{\lambda}_L$ has been determined, the method uses original cross-section buckling curves to determine a (local) penalty factor χ_L that decreases the plastic capacity taken as reference owing to buckling effects and imperfections. These various steps are illustrated on Figure 10.

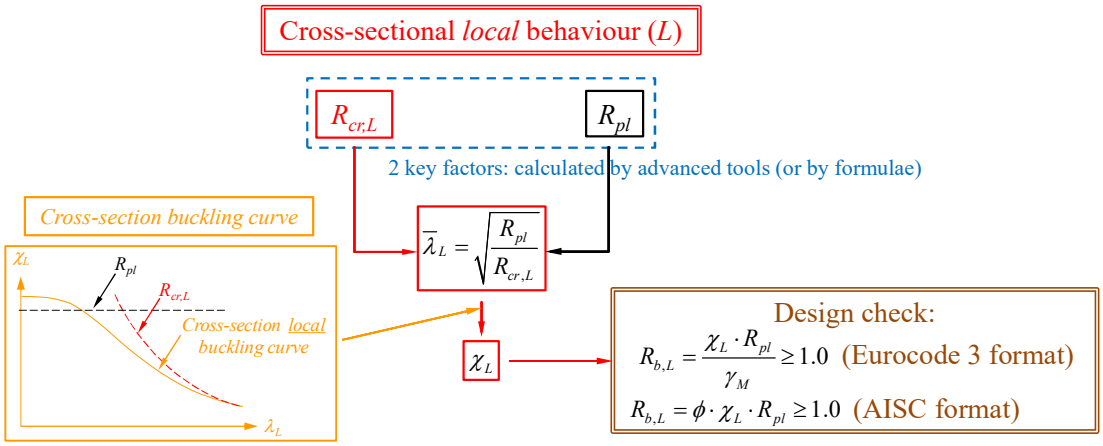

Figure 10: O.I.C. design flow chart for cross section resistance.

It is important to note that some coefficients may or shall be calculated by tools – the O.I.C. approach is among the first ones to offer the possibility to rely on numerical tools for the calculation of key coefficients. In Figure 10, $R_{cr,L}$ stand as the load ratio by which the initial loading shall be multiplied to reach the (local) critical state; $R_{cr,L}$ therefore corresponds to an L.B.A. calculation. $R_{b,L}$ is the factor by which the initial loading shall be multiplied to reach the ultimate section capacity, and is therefore obtained through a G.M.N.I.A. computation. Use of such load factors or load ratios is made necessary to address combined loading situations through the same simple concept. In situations where a simple load case is considered, *R*-ratios can usefully be substituted by their internal forces counterparts (e.g., under compression *N*, $N_{cr,L}$ and $N_{b,L}$ can be used in lieu of $R_{cr,L}$ and $R_{b,L}$, respectively). Within the present study and in an effort to ensure accuracy and consistency with the sources of the results presented, ABAQUS was used to provide numerically-computed values of $R_{cr,L}$ and $R_{b,L}$. As for R_{pl} factor, which represents the load factor to reach the plastic capacity (all fibers yielded), a separate fiber-based cross-section model was programmed specifically, with the ability to account for (i) the section's accurate geometry and (ii) a lower yield stress in the H.A.Z. for welded sections. Accordingly, plastic capacities through factor R_{pl} were quite accurately taken into account. Further details and background information on the O.I.C. approach may be found in (Boissonnade et al. 2017; Gérard et al. 2021; Li et al. 2022; Coderre 2022).

As a particular point of the proposed approach, the selection of an appropriate buckling curve is essential. Observations showed that there cannot be a unique, safe-sided curve unless it stands as a (very) conservative one. Exceedingly simple, this was deemed inappropriate, inaccurate and uneconomical and specific analyses were led to understand how a series of cross-section

buckling curves should be defined, i.e., identify parameters responsible for different resistance responses beyond the ones already involved in the O.I.C. approach.

This led to identifying a geometrical parameter, denoted as γ (see Eqs. (7) and (8)), to be responsible for the scatter in observed results. Therefore, a series of buckling curves with a dependency on γ have been established and are detailed in Section 3.2 for extruded sections and along Section 3.3 for welded shapes.

$$\gamma_{\mathrm{E}} = \left(\frac{h}{t_{\mathrm{w}}}\right)^{2} \cdot \left(\frac{b}{t_{\mathrm{f}}}\right) \cdot \left(\frac{t_{\mathrm{w}}}{t_{\mathrm{f}}}\right) \quad \textit{for extruded shapes} \tag{7}$$

$$\gamma_{\mathrm{W}} = \left(\frac{h}{t_{\mathrm{w}}}\right)^{0.8} \cdot \left(\frac{b}{t_{\mathrm{f}}}\right) \cdot \left(\frac{t_{\mathrm{w}}}{t_{\mathrm{f}}}\right) \cdot 10^{-3} \quad \textit{for welded shapes} \tag{8}$$

3.2 Design proposals for extruded sections

In a first step, O.I.C.-based design equations have been developed for extruded I-shapes. For compact sections with $\bar{\lambda}_{\mathrm{L}} < \lambda_0$ where λ_0 is a reference (limit) slenderness, a strain-based approach is suggested so as to better account for strain hardening resistance reserves. A relationship between $\bar{\lambda}_{\mathrm{L}}$ and the ratio $\varepsilon_{peak} / \varepsilon_y$ is first established, where ε_{peak} is the strain level at peak load and ε_y is the strain at $\sigma_{0.2}$. This ratio stands as a sound indicator of the potential benefits from the pronounced non-linear material response of aluminium alloys, and allows, through a 2nd step that links $\varepsilon_{peak} / \varepsilon_y$ to χ_{L}, to provide resistance predictions higher than the usual, conventional plastic capacity. Figure 11a and Figure 11b illustrate this strain-based approach for compact aluminium I-shapes under major axis bending moment M_{y}.

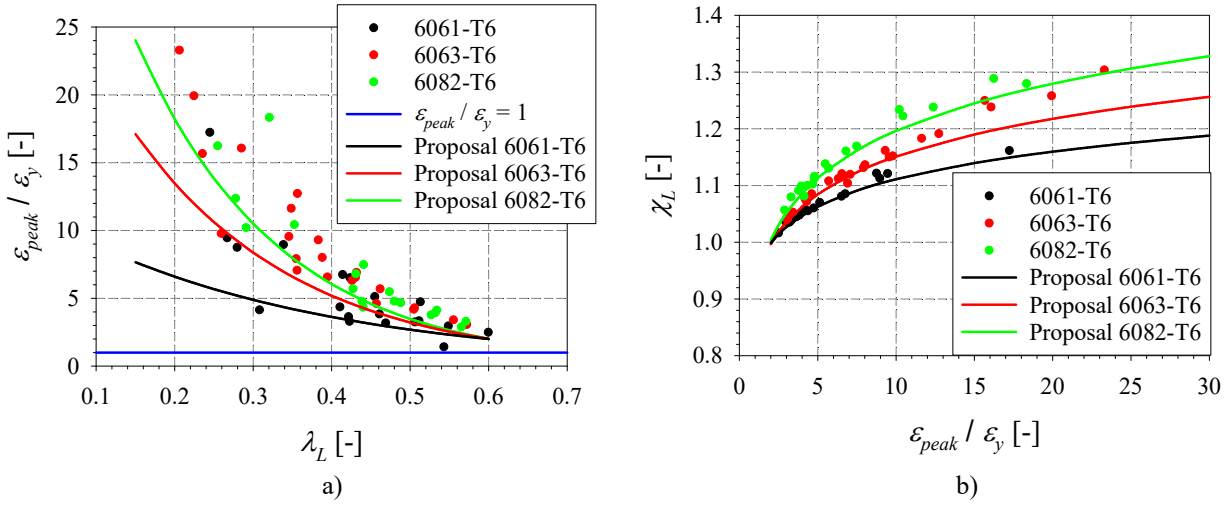

Figure 11: Principle of two-step procedure for $\lambda_L \leq \lambda_0$ (major-axis bending cases).

For more slender shapes, i.e., $\bar{\lambda}_{\mathrm{L}} > \lambda_0$, the proposed approach more classically relies on a direct $\bar{\lambda}_{\mathrm{L}} - \chi_{\mathrm{L}}$ approach, through a so-called "modified Ayrton-Perry" approach (Ayrton and Perry 1886; Boissonnade et al. 2017; Li et al. 2022) – cf. Table 6 for definitions and coefficients. In the proposed equations, parameter α_{L} stands as a general (cross-sectional) imperfection factor while δ aims at specifically accounting for plate post-buckling effects; note that both α_{L} and δ are functions of geometrical parameter γ.

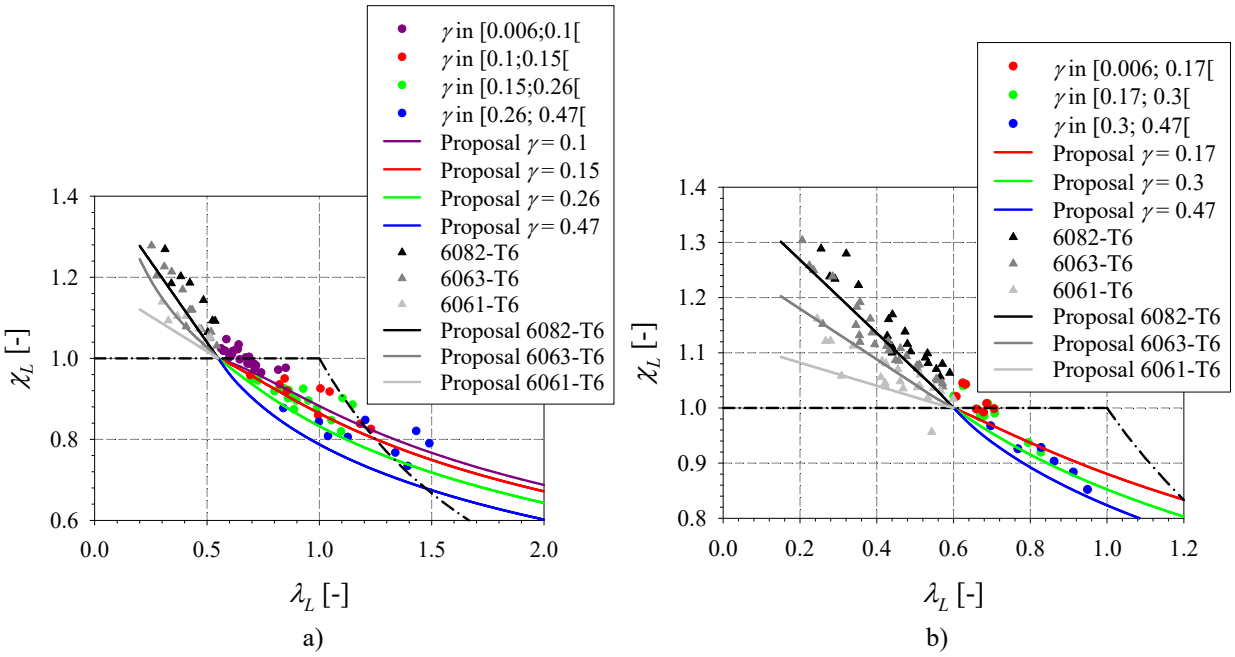

Figure 12: Performance of proposed approach for extruded sections – a) Compression – b) Major-axis bending.

Figure 12a and Figure 12b propose a series of results over the entire $\bar{\lambda}_L$ domain, i.e., for compact and slender shapes, for the cases of simple compression N and major-axis bending M_y. It can be observed that the proposed approach provides quite accurate yet safe resistance estimates when compared to the reference F.E. data – note however that the figures only plot a few lower bound curves of the O.I.C. proposal (since the buckling curves are γ-dependent) while each individual data point possesses it own unique γ value, so that the curves plotted are usually safe-sided for the interval of γ they correspond to.

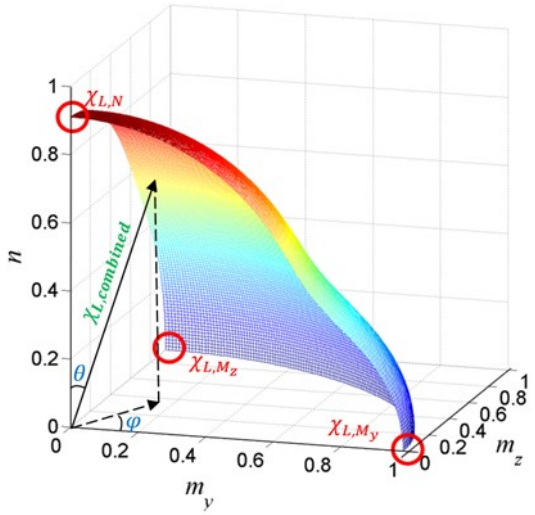

Figure 13: 3D resistance surface.

Table 6: Design proposal for aluminium cross-sections under simple load cases.

Manufacturing Types	Load cases	Compression N	Major-axis bending M_y	Major-axis bending M_z
Extruded cross-sections		For $\overline{\lambda}_{L,N} \le \lambda_0 = 0.55$:	For $\overline{\lambda}_{L,My} \le \lambda_0 = 0.60$:	For $\overline{\lambda}_{L,Mz} \le \lambda_0 = 0.60$:
	Alloy 6063-T6	$\chi_{L,N} = -0.067 - 0.24 \cdot \ln(\overline{\lambda}_{L,N})$	$\chi_{L,My} = 1.27 - 0.46 \cdot \overline{\lambda}_{L,My}$	$\chi_{L,Mz} = 1.22 - 0.35 \cdot \overline{\lambda}_{L,Mz}$
	Alloy 6061-T6	$\chi_{L,N} = 1.19 - 0.35 \cdot \overline{\lambda}_{L,N}$	$\chi_{L,My} = 1.12 - 0.21 \cdot \overline{\lambda}_{L,My}$	$\chi_{L,Mz} = 1.08 - 0.14 \cdot \overline{\lambda}_{L,Mz}$
	Alloy 6082-T6	$\chi_{L,N} = 1.44 - 0.79 \cdot \overline{\lambda}_{L,N}$	$\chi_{L,My} = 1.40 - 0.66 \cdot \overline{\lambda}_{L,My}$	$\chi_{L,Mz} = 1.22 - 0.36 \cdot \overline{\lambda}_{L,Mz}$
	Ayrton-Perry format	For $\overline{\lambda}_{L,N} > \lambda_0 = 0.55$: $\phi_L = 0.5 \cdot \left(1 + \alpha_L \cdot \left(\overline{\lambda}_{L,N} - \lambda_0\right) + \overline{\lambda}_{L,N}^{\delta}\right)$ $\chi_{L,N} = \frac{\beta}{\phi_L + \sqrt{\phi_L^2 - \overline{\lambda}_{L,N}^{\delta}}}$ $\alpha_L = 0.01 + 0.25\gamma_E$ $\delta = 0.4 + 0.3\gamma_E$	For $\overline{\lambda}_{L,My} > \lambda_0 = 0.60$: $\phi_L = 0.5 \cdot \left(1 + \alpha_L \cdot \left(\overline{\lambda}_{L,My} - \lambda_0\right) + \overline{\lambda}_{L,My}^{\delta}\right)$ $\chi_{L,My} = \frac{\beta}{\phi_L + \sqrt{\phi_L^2 - \overline{\lambda}_{L,My}^{\delta}}}$ $\alpha_L = 0.01 + 0.18\gamma_E$ $\delta = 0.3 - 0.1\gamma_E$	For $\overline{\lambda}_{L,Mz} > \lambda_0 = 0.60$: $\phi_L = 0.5 \cdot \left(1 + \alpha_L \cdot \left(\overline{\lambda}_{L,Mz} - \lambda_0\right) + \overline{\lambda}_{L,Mz}^{\delta}\right)$ $\chi_{L,Mz} = \frac{\beta}{\phi_L + \sqrt{\phi_L^2 - \overline{\lambda}_{L,Mz}^{\delta}}}$ $\alpha_L = 0.2\gamma_E$ $\delta = 0.4 - 0.2\gamma_E$
Welded Cross-sections		For $\overline{\lambda}_{L,N} \le \lambda_0 = 0.50$:	For $\overline{\lambda}_{L,My} \le \lambda_0 = 0.45$:	For $\overline{\lambda}_{L,Mz} \le \lambda_0 = 0.60$:
	Alloy 6061-T6	$\chi_{L,N} = 1.12 - 0.24 \cdot \overline{\lambda}_{L,N}$	$\chi_{L,My} = 1.12 - 0.27 \cdot \overline{\lambda}_{L,My}$	$\chi_{L,Mz} = 1.10 - 0.16 \cdot \overline{\lambda}_{L,Mz}$
	Alloy 6082-T6	$\chi_{L,N} = 1.37 - 0.73 \cdot \overline{\lambda}_{L,N}$	$\chi_{L,My} = 1.18 - 0.40 \cdot \overline{\lambda}_{L,My}$	$\chi_{L,Mz} = 1.24 - 0.40 \cdot \overline{\lambda}_{L,Mz}$
	Ayrton-Perry format	For $\overline{\lambda}_{L,N} > \lambda_0 = 0.50$: $\phi_L = 0.5 \cdot \left(1 + \alpha_L \cdot \left(\overline{\lambda}_{L,N} - \lambda_0\right) + \overline{\lambda}_{L,N}^{\delta}\right)$ $\chi_{L,N} = \frac{\beta}{\phi_L + \sqrt{\phi_L^2 - \overline{\lambda}_{L,N}^{\delta}}}$ $\alpha_L = 0.04 + 0.65\gamma_W$ $\delta = 0.5 - 1.50\gamma_W \ge 0$	For $\overline{\lambda}_{L,My} > \lambda_0 = 0.45$: $\phi_L = 0.5 \cdot \left(1 + \alpha_L \cdot \left(\overline{\lambda}_{L,My} - \lambda_0\right) + \overline{\lambda}_{L,My}^{\delta}\right)$ $\chi_{L,My} = \frac{\beta}{\phi_L + \sqrt{\phi_L^2 - \overline{\lambda}_{L,My}^{\delta}}}$ $\alpha_L = 0.06 + 0.55\gamma_W$ $\delta = 1.4 - 1.5\gamma_W$	For $\overline{\lambda}_{L,Mz} > \lambda_0 = 0.60$: $\phi_L = 0.5 \cdot \left(1 + \alpha_L \cdot \left(\overline{\lambda}_{L,Mz} - \lambda_0\right) + \overline{\lambda}_{L,Mz}^{\delta}\right)$ $\chi_{L,Mz} = \frac{\beta}{\phi_L + \sqrt{\phi_L^2 - \overline{\lambda}_{L,Mz}^{\delta}}}$ $\alpha_L = 0.13 - 0.2\gamma_W$ $\delta = 0.15 - 1.4\gamma_E$

As for combined load cases, the proposed O.I.C. approach relies on the definition of a 3D resitance surface (see Figure 13), where each axis refers to a relative amount of an internal force – either relative axial compression n or relative major or minor-axis bending moments m_y and m_z, cf. Eqs. (2) – (4). This surface is such that any load combination leading to a point below this surface indicates that the design under the considered forces is safe-sided, while a point lying on this surface means that maximum resistance is just reached – obviously, loading points outside/above this surface denotes that capacity is exceeded and that loading shall be reduced. A spherical system of coordinates shows appropriate in this context, and use of angles θ and φ as defined in Eqs. (5) and (6) is useful and efficient. In this respect, Eq. (9) may suitably be used for combined load cases. In Eq. (9), q factors allow for adjustments in the proposed resistance surface at both (i) the overall level (q_1 affects the general shape of the 3D surface), or (ii) a more localized level, through factors q_2 to q_6 which enable local tuning of the surface where a given internal force is dominant. For example, q_2 locally modifies the shape of the resistance surface when axial compression is dominant. The q factors have been optimised for providing the best compromise between accuracy, simplicity and safety, and their proposed values are summarized in Table 7.

$$\chi_{\mathrm{L,combined}} = \left[\left(\chi_{\mathrm{L,N}} \cdot \cos^{q_2} \theta \right)^{q_1} + \left(\chi_{\mathrm{L,M_y}} \cdot \sin^{q_3} \theta \cdot \cos^{q_4} \varphi \right)^{q_1} + \left(\chi_{\mathrm{L,M_z}} \cdot \sin^{q_5} \theta \cdot \sin^{q_6} \varphi \right)^{q_1} \right]^{\frac{1}{q_1}} \quad (9)$$

Table 7: O.I.C. design factors for combined load cases.

q factors	q_1	q_2	q_3	q_4	q_5	q_6
Extruded cross-sections	9	0.19	1.2	0.13	3.5	8
Welded cross-sections	5	0.80	1.3	0.6	2.2	3

Figure 14a and Figure 14b summarize the 1 170 F.E. results for various load combinations against which the accuracy and safety of the proposed approach can be tested. Figure 14a examines the overall accuracy of the O.I.C. proposal through plotting the frequencies of the $\chi_{\mathrm{L,O.I.C}} / \chi_{\mathrm{L,F.E.}}$ ratio along various accuracy intervals. Ratios < 1.0 denote safe O.I.C. resistance predictions, while ratios above unity point towards unsafe estimates. As can be observed, the proposed design approach here again provides excellent results, precise and safe-sided, with a very good consistency level as indicated by a narrow standard deviation. Figure 14b proposes to split the results by load cases, and allows to identify the situations where predictions are either unsafe or over-conservative. A vast majority of the results fall in between the targeted $\chi_{\mathrm{L,O.I.C}} / \chi_{\mathrm{L,F.E.}}$ ratios, which are highlighted by the green and the red dotted lines. The prediction for results from combined load cases with $N + M_y + M_z$ generally tend to be a bit unconservative, with some results below the 1.0 line. Most of the results are quite close to the 1.0 line and, therefore, are not so unconservative – this shall easily be compensated by usual safety factor values, see final design step in Figure 10.

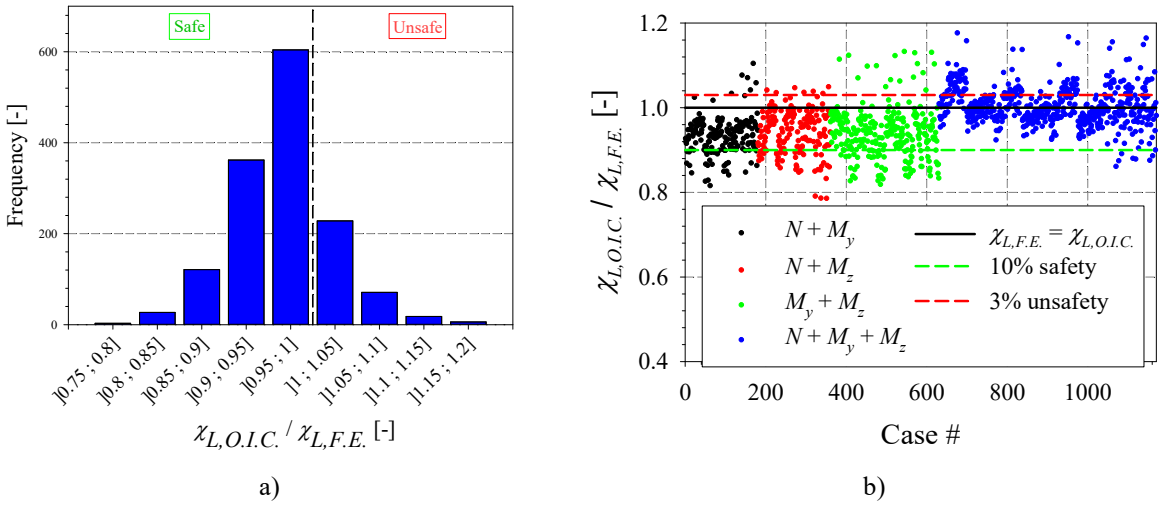

Figure 14: a) Accuracy of proposal for combined load cases (extruded sections, all cases included) – b) Performance of proposal based on load cases.

For a more detailed analysis of the results, Table 8 compiles statistical results obtained with the O.I.C. design proposal for extruded sections, sorted per load combination. It shows that for simple load cases, the design proposal presents a great accuracy. All three simple load cases have an average close to 1.0, and a very low standard deviation, the highest being as low as 3.0% for pure compression. All standard deviation values reported are excellent, and virtually no problematical unsafe result is reported – only very few values are indeed higher than 1.05. The most conservative value for simple load cases is reported as 0.86 for pure compression, which is still considered as fairly accurate.

For combined load cases, Table 8 also shows that the proposal meets a very good accuracy. The average $\chi_{L,O.I.C} / \chi_{L,F.E.}$ ratios range from 0.93 to 1.0 and the highest standard deviation is only 6.0%, meaning that the results are very consistent and continuous. Results for $N + M_z$ cases present the best performance, and, as expected, the most complex $N + M_y + M_z$ combinations are associated with the "worst" performances: even if it has a really low standard deviation of 4.5% and an average of exactly 1.0, almost half of the results (48%) have a value higher than 1.0. However, this number decreases drastically to 14% for values over 1.05, meaning that almost all the results are located between 1.0 and 1.05, which is considered accurate. As mentioned previously, a safety factor will eventually complement the proposal, shifting the unconservative results towards safer results.

The overall performance of the design proposal for extruded sections is therefore very satisfactory. Including all results, the average $\chi_{L,O.I.C} / \chi_{L,F.E.}$ ratio is 0.97, with a standard deviation of 5.6%, meaning that the vast majority of the results are grouped just under a value of 1.0. Indeed, only 10% of all the results are below 0.9, and only 7% are higher than 1.05. When looking at unsafe values over 1.1, this value drops to less than 2%.

Table 8: Statistical results of proposal for extruded sections based on load combination.

Load case	N	M_y	M_z	$N + M_y$	$N + M_z$	$M_y + M_z$	$N + M_y + M_z$	All
Average	0.97	0.97	0.93	0.93	0.94	0.94	1.00	0.97
Maximum	1.01	1.06	1.02	1.10	1.05	1.13	1.18	1.18
Minimum	0.86	0.90	0.89	0.82	0.79	0.82	0.86	0.79
C.O.V.	0.03	0.02	0.03	0.05	0.06	0.06	0.05	0.06
Values < 0.8	0	0	0	0	3 (2%)	0	0	3 (0%)
Values < 0.9	3 (3%)	0	4 (4%)	34 (19%)	39 (22%)	64 (24%)	7 (1%)	151 (10%)
Values > 1.0	7 (8%)	4 (4%)	1 (1%)	9 (5%)	20 (11%)	25 (9%)	257 (48%)	323 (22%)
Values > 1.05	0	1 (1%)	0	4 (2%)	0	15 (6%)	75 (14%)	95 (7%)
Values > 1.1	0	0	0	1 (1%)	0	8 (3%)	15 (3%)	24 (2%)
Values > 1.2	0	0	0	0	0	0	0	0
Total cases	90	90	90	180	180	270	540	1440

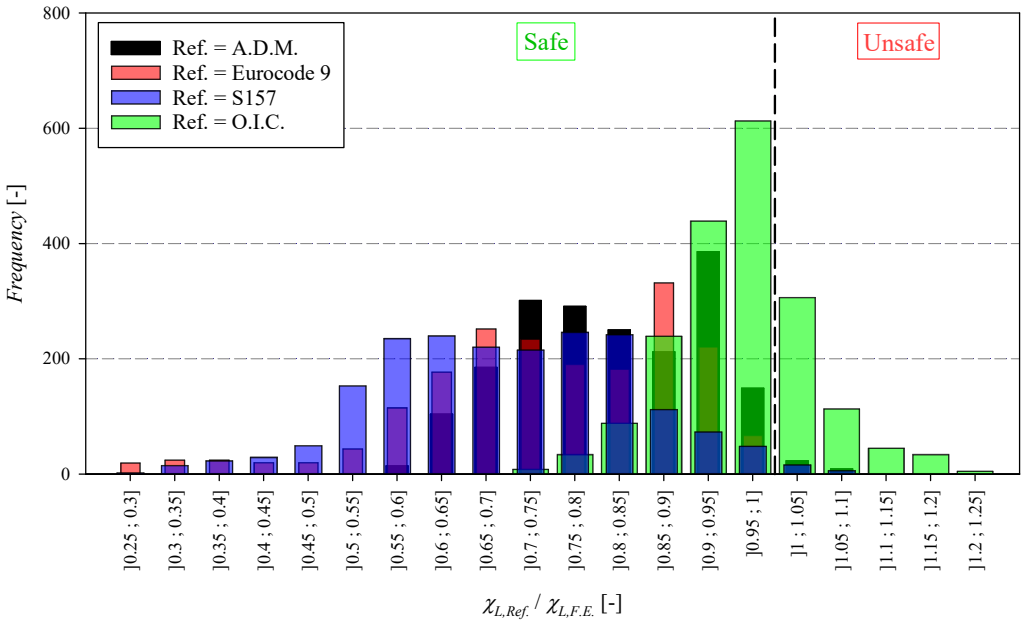

Figure 15: Performance of proposed approach vs existing ones (Eurocode 9, A.D.M. and S157) for combined load cases – extruded sections.

The pertinence of the proposed approach was also tested against existing design approaches, namely the the European Standards (Eurocode 9 Part 1-1 (European Committee for Standardization 2007)), the American Standards (cf. Aluminum Design Manual (Aluminum Association 2020)) and the Canadian Standards (CSA S157-17 (Canadian Standards Association 2017)). In this respect, reduction factors χ_L – which stand as a direct meaure of resistance – have been calculted as recommended in these standards and compared to the proposed approach and to the reference F.E. results. Figure 15 first proposes summary histograms of frequencies of the $\chi_{L,Ref.} / \chi_{L,F.E.}$ ratio, where $\chi_{L,Ref.}$ sucessively refers to one of the standards or to the O.I.C. proposal. Overall, this figure shows that (i) the O.I.C. approach proposes, by far, the best resistance predictions both regarding accuracy, consistency and safety and that (ii) all other

design approaches yield quite conservative resistance estimates, where the predicted resistances can even be doubled sometimes.

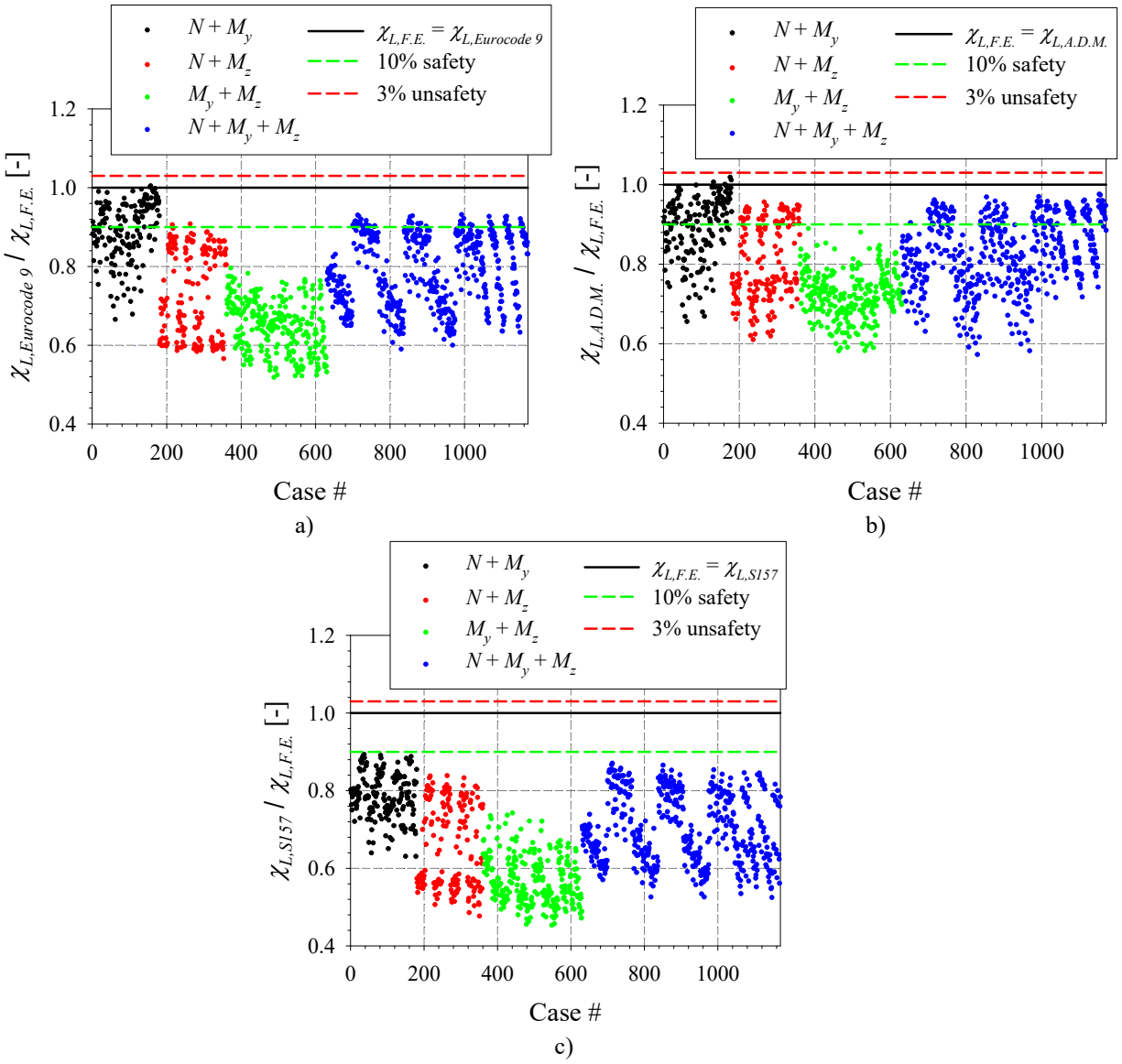

Figure 16: Performance of proposed approach vs existing ones (Eurocode 9, A.D.M. and S157) for combined load cases (extruded sections) – a) Results for Eurocode 9 – b) Results for A.D.M. – c) Results for S157.

Further, Figure 16a to Figure 16c propose a load case-dependent view of the same results, for each standard. It is observed that Eurocode 9 generally underestimates the carrying capacity for every combined loading situation, in particular when M_y and/or M_z are dominant. In average, Eurocode 9 provides some 30% over-conservatism, and leads to quite scattered predictions. Similarly, A.D.M. specifications lead to quite over-safe resistance estimates, yet a little less conservative than Eurocode 9 and still very scattered. S157 is seen to lead to the worst results in terms of accuracy; the results are also very scattered and never get any closer than 10% on the safe side, which is rather uneconomical.

All these results ought to be compared to the ones reached for the O.I.C. proposal presented on Figure 14b, to emphasize how significantly better the proposed approach stands in all relevant aspects of accuracy, consistency and economy.

3.3 Design proposals for welded sections

Design equations for welded sections have been derived in the same way as for extruded shapes, namely with (i) a proposal based on the $\varepsilon_{peak} / \varepsilon_y$ ratio for the most compact shapes, (ii) a generalized Ayrton-Perry format for the slender shapes and (iii) the definition of a 3D resistance surface for combined load cases. Also, for each load case, a scatter in the results was found associated with the various dimensions of the sections, so that a similar γ_W factor was defined as in Eq. (8), in order to propose a series of (local) buckling curves.

Figure 17a illustrates the results obtained for this proposal for welded sections in compression, while Figure 17b proposes results for sections bent about the major-axis M_y. As can be observed, the O.I.C. proposal provides very good resistance predictions in comparison to the reference F.E. data points. Further, Figure 18a plots a statistical summary of the results obtained for combined load cases; here again, the O.I.C.-based approach is seen to lead to accurate, consistent and generally safe-sided predictions. In Figure 18b, the individual load case results are detailed, and it is again observed that the proposed approach gives quite satisfactory results, whatever the load case. Especially for the most complex $N+M_y+M_z$ cases, the performance of the proposed approach is seen very good.

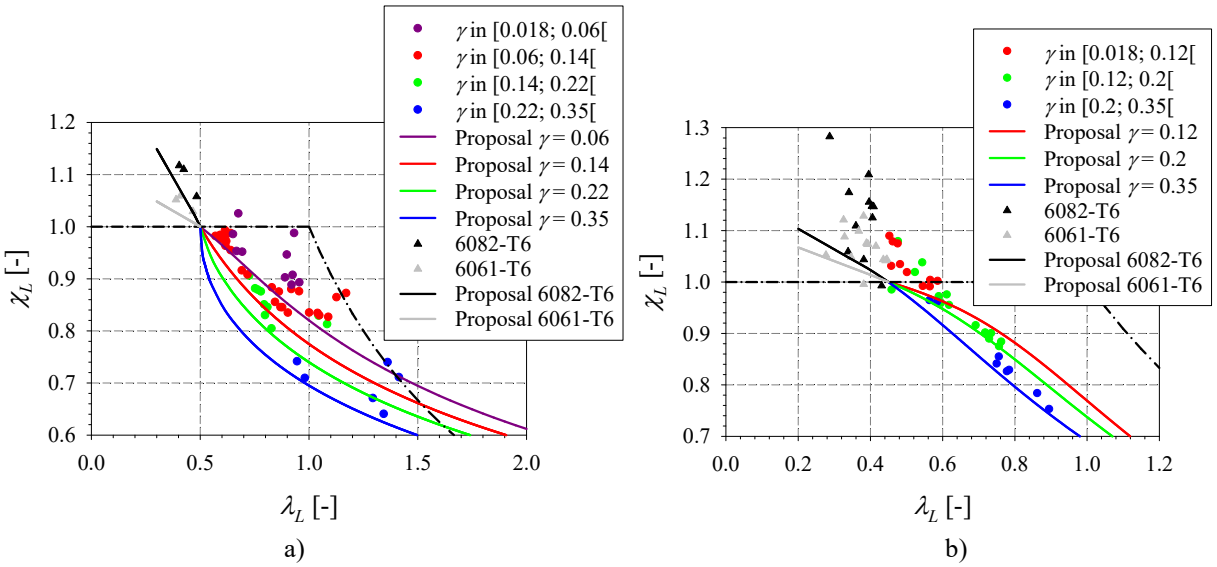

Figure 17: Performance of proposed approach for welded sections – a) Compression – b) Major-axis bending.

Table 9 gives further details on how the results are distributed per load case with relevant statistical data. Overall, the O.I.C. proposal is 5% conservative on the 928 F.E. reference cases considered, with a C.O.V. lower than 9%, which is excellent. All average and C.O.V. values can be seen to be outstanding, given the complexity of the problem and the many variables considered (very different geometries, alloys, load conbinations, etc.). The proposal is also seen to provide very little over-safe predictions (less than 4% of the 928 results exceed 20% over-conservatism) as well as limited unsafe resistance estimates (6% of the results are over the 10% limit beyond which usual safety factors compensate for unsafe predictions).

Table 9: Statistical results of proposal for welded sections based on load combination.

Load case	N	M_y	M_z	$N + M_y$	$N + M_z$	$M_y + M_z$	$N + M_y + M_z$	All
Average	0.95	0.96	0.95	0.94	0.94	0.92	0.97	0.95
Maximum	1.01	1.02	0.99	1.15	1.19	1.18	1.21	1.21
Minimum	0.87	0.83	0.9	0.78	0.74	0.71	0.78	0.71
C.O.V.	0.033	0.042	0.023	0.081	0.099	0.098	0.092	0.087
Values < 0.8	0	0	0	2 (2%)	14 (12%)	22 (13%)	1 (0%)	39 (4%)
Values < 0.9	5 (9%)	6 (10%)	0	29 (25%)	32 (28%)	74 (43%)	90 (26%)	236 (25%)
Values > 1.0	3 (5%)	6 (10%)	0	24 (21%)	23 (20%)	33 (19%)	112 (32%)	201 (22%)
Values > 1.05	0	0	0	15 (13%)	13 (11%)	17 (10%)	58 (17%)	103 (11%)
Values > 1.1	0	0	0	7 (6%)	9 (8%)	9 (5%)	35 (10%)	60 (6%)
Values > 1.2	0	0	0	0	0	0	5 (1%)	5 (1%)
Total cases	58	58	58	116	116	174	348	928

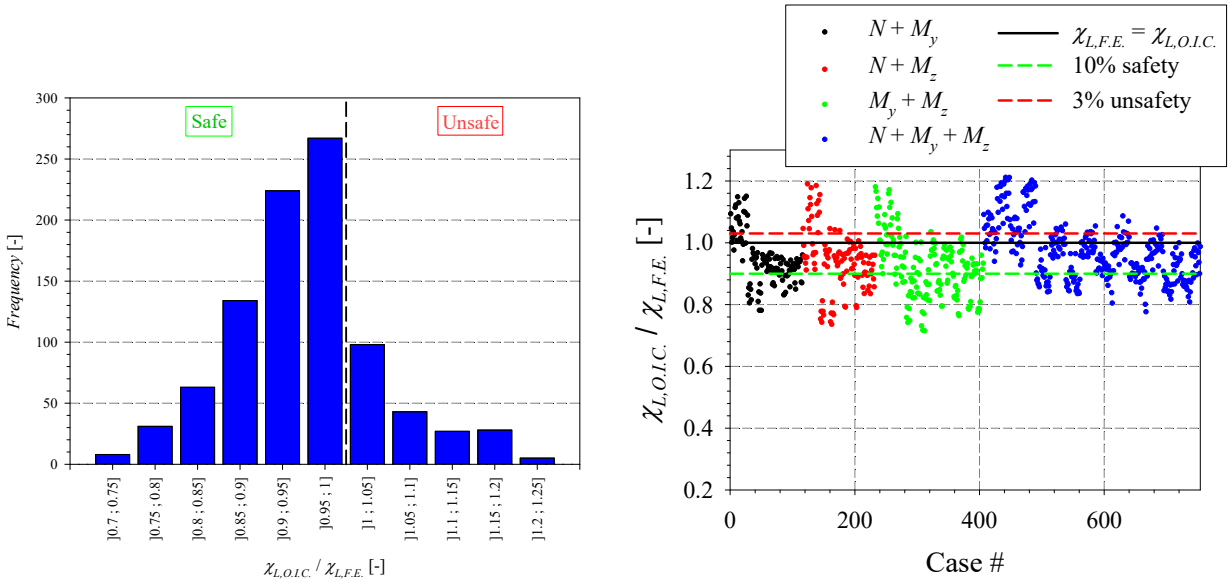

a) b)

Figure 18: a) Accuracy of proposal for combined load cases (welded sections, all cases included) – b) Performance of proposal based on load cases.

Similarly to extruded sections, the histograms in Figure 19 further illustrate how much of an improvement the proposed O.I.C. approach can represent compared to existing design provisions. It is in particular interesting to note that (i) other design approaches provide very scattered, inconsistent predictions and that (ii) some results show extremely conservative: as an example, one can cite the non-negligible amount of results from Eurocode 9 or S157 having $\chi_{L,Ref.} / \chi_{L,F.E.}$ ratios in the vicinity of 0.33 or lower, which indicates that the failure loads predicted by these codes may actually be multiplied by at least a factor 3 to reach the reference ultimate capacities of the F.E. models.

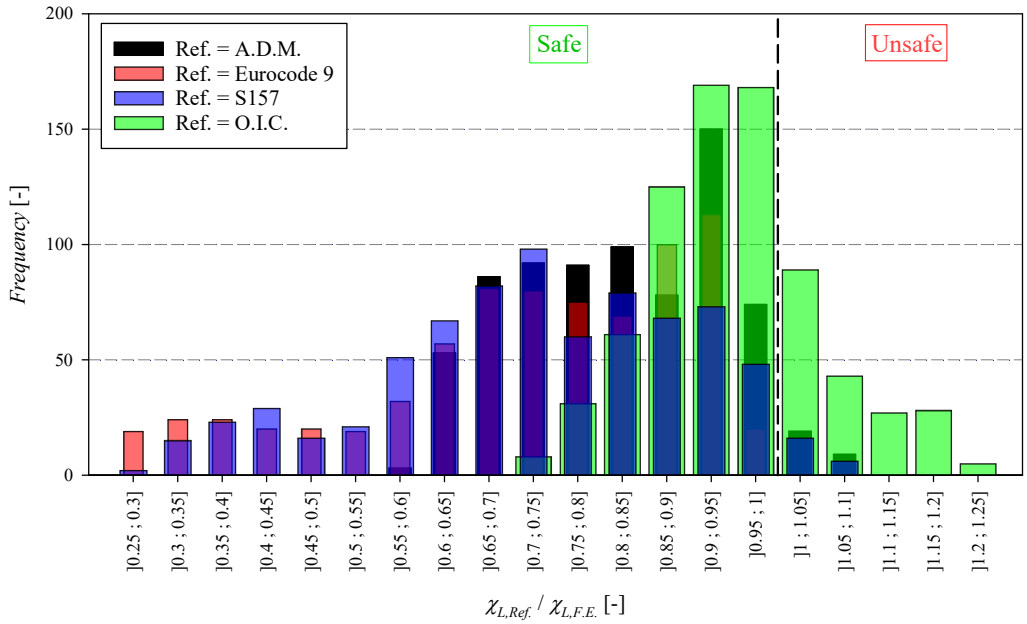

Figure 19: Performance of proposed approach vs existing ones (Eurocode 9, A.D.M. and S157) for combined load cases – welded sections.

As a complement to Figure 19, Figure 20 breaks down these results per individual load cases (only combined load cases are reported on this figure), and allows to further illustrate that (i) all existing code proposals provide extremely conservative, over-safe resistance predictions and that (ii) they all lead to very scattered results, although the A.D.M. approach is seen to be the best among them. When compared to Figure 18b, it further illustrates that the O.I.C.-based proposal brings significant improvements in accuracy/economy, consistency and safety.

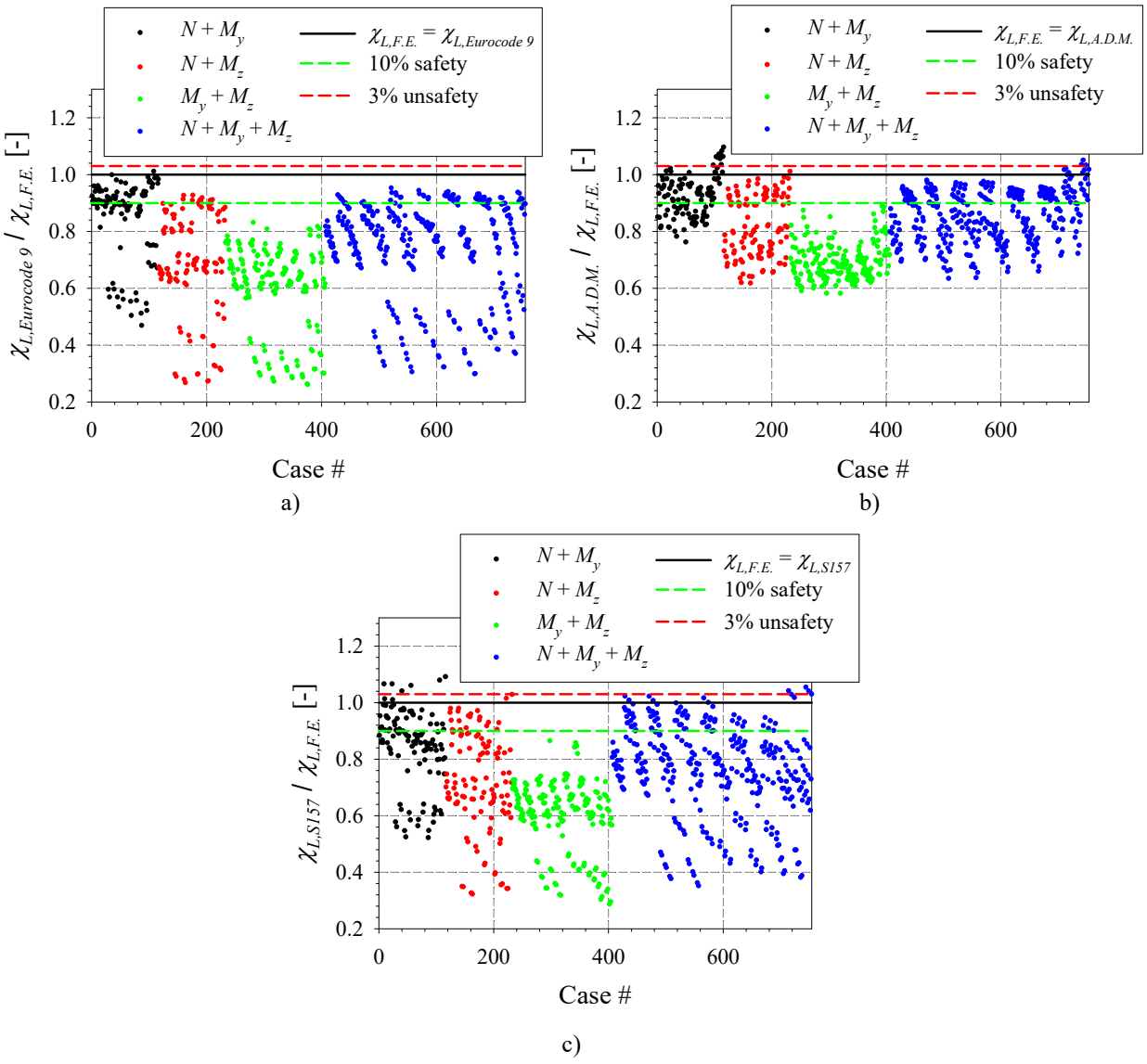

Figure 20: Performance of proposed approach vs existing ones (Eurocode 9, A.D.M. and S157) for combined load cases (welded sections) – a) Results for Eurocode 9 – b) Results for A.D.M. – c) Results for S157.

4. Conclusions

This paper presented an original O.I.C.-based approach for the design of aluminium I-shaped sections under simple or combined load cases. For simple load cases, this design proposal relies on a specific, strain-based 2-step approach for predicting the resistance of compact aluminium shapes, and on a so-called "extended Ayrton-Perry" format for the most slender shapes, both providing direct capacity estimates. For combined loading situations, the suggested approach relies on a 3D resistance surface and on the use of a system of spherical coordinates. Advanced non-linear shell F.E. models were also developed then validated against more than 15 test results. Then, some 2 300 numerical simulations were performed to gather a large dataset of reference results that were used to investigate the adequacy of the proposed design approach. The latter is proved very satisfactory in terms of accuracy, economy, safety and consistency. Compared to existing design provisions for aluminium profiles in Eurocode 9, in the American A.D.M. recommendations or in the Canadian Standards S157, the suggested approach is seen to

significantly improve design predictions, making this proposal an interesting candidate for an alternative design proposal intended at practitioners.

5. References

Abaqus (2011). "Abaqus 6.11:" *Dassault Systemes Simulia Corporation, Providence, RI, USA*.

Aluminum Association (2020). Aluminum Design Manual: 2020, Aluminum Association, Washington, D.C.

Ayrton, W.E. and Perry, J. (1886). "On struts:" *The Engineer*, Vol. 62.

Bathe, K. J. (2016). "Finite Element Procedures", 2nd Edition, Prentice Hall, Pearson Education.

Beyer, A. (2017). *On the Design of Members with Open Cross Sections Subject to Combined Axial Compression, Bending and Torsion*, PhD thesis, Lorraine University.

Boissonnade, N., Hayeck, M., Saloumi, E. and Nseir, J. (2017). "An Overall Interaction Concept for an alternative approach to steel members design:" *Journal of Constructional Steel Research*, Vol. 135, pp. 199–212.

Canadian Standards Association (2017). CSA S157-17: Strength design in aluminum.

Coderre, T. (2022). *Development of an alternative design method for aluminium open cross-sections using the Overall Interaction Concept*, MSc Thesis, Civil and Water Engineering Department, Laval University.

European Committee for Standardization (2007). Eurocode 9: Design of aluminium structures - Part 1-1: General structural rules, Commission of the European Community, Brussels, Belgium.

Extrudex Aluminium Inc. (2020). Standard Shapes Catalogue.

Gagné, A.-S. (2022). *Design of stainless steel welded I-sections by means of the Overall Interaction Concept*, MSc Thesis, Université Laval, Québec, Canada.

Gagné, A.-S., Gérard, L. and Boissonnade, N. (2020). "Design of stainless steel cross-sections for simple load cases with the O.I.C.:" *Journal of Constructional Steel Research*, Vol. 168, p. 105936.

Gérard, L., Li, L., Kettler, M. and Boissonnade, N. (2019). "Recommendations on the geometrical imperfections definition for the resistance of I-sections:" *Journal of Constructional Steel Research*, Vol. 162, p. 105716.

Gérard, L., Li, L., Kettler, M. and Boissonnade, N. (2021). "Steel I-sections resistance under compression or bending by the Overall Interaction Concept:" *Journal of Constructional Steel Research*, Vol. 182, p. 106644.

Guo, Z.T. (1989). “Bending and Torsion of Thin-Walled Members:” Chinese Architectural and Industrial publishing House Beijing.

Hill, H.N. (1944). Determination of stress-strain relations from “offset” yield strength values.

Kristensen, O.H.H. and Moan, T. (1999). “Ultimate strength of aluminium plates under biaxial loading:” *Proc., Fifth Int. Conf. on Fast Sea Transportation, Society of Naval Architects and Marine Engineers*.

Li, L., Gérard, L., Kettler, M. and Boissonnade, N. (2022). “The Overall Interaction Concept for the design of hot-rolled and welded I-sections under combined loading:” *Thin-Walled Structures*, Vol. 172, p. 108623.

Mazzolani, F. (1994). Aluminium Alloy Structures, CRC Press.

Metra Aluminium Inc. (2019). Catalogue FR - Profilé en “I” avec rayons.

Ramberg, W. and Osgood, W.R. (1943). Description of stress-strain curves by three parameters.

Rigo, P., Sarghiuta, R., Estefen, S., Lehmann, E., Otelea, S.C., Pasqualino, I., Simonsen, B.C., Wan, Z. and Yao, T. (2003). “Sensitivity analysis on ultimate strength of aluminium stiffened panels:” *Marine Structures*, Vol. 16, No. 6, pp. 437–468.

Riks, E. (1979) "An Incremental Approach to the Solution of Snapping and Bucking Problems," International Journal of Solids and Structures, Vol. 15, pp. 529-551.

Sapa Inc. (2008). Hydro Catalog Standard Shapes.

Yuan, H.X., Wang, Y.Q., Chang, T., Du, X.X., Bu, Y.D. and Shi, Y.J. (2015). “Local buckling and postbuckling strength of extruded aluminium alloy stub columns with slender I-sections:” *Thin-Walled Structures*, Vol. 90, pp. 140–149.

Zha, Y. and Moan, T. (2001). “Ultimate strength of stiffened aluminium panels with predominantly torsional failure modes:” *Thin-Walled Structures*, Vol. 39, No. 8, pp. 631–648.

Zha, Y. and Moan, T. (2003). “Experimental and Numerical Prediction of Collapse of Flatbar Stiffeners in Aluminum Panels:” *Journal of Structural Engineering*, Vol. 129, No. 2, pp. 160–168.